

Continuous Shape Sensitivity Equation Method for the $k - \epsilon$ Model of Turbulence

R. Di Caro * A. Hay † S. Etienne ‡ and D. Pelletier §

Département de Génie Mécanique, Ecole Polytechnique de Montréal
Montréal (Québec), CANADA, H3C 3A7

A Continuous Shape Sensitivity Equation (CSE) method is presented for shape parameters and applied turbulent wall-bounded flows computed using the standard $k - \epsilon$ turbulence model with wall functions. Computations are done with an adaptive finite-element code. This paper is an extension of previous works on sensitivity analysis of laminar flows for shape parameters and wall-bounded turbulent flows for value parameters. The differentiation of two-velocity scale wall functions, accounting for their complex dependencies on boundary shape parameters, is presented in details. Flow and sensitivity solutions are first verified on a problem with a closed form solution using the Method of the Manufactured Solution. The problem allows for the Verification of the wall functions and their sensitivities with respect to shape parameters. The method is then applied to turbulent flows around a square obstacle in proximity of a solid wall to investigate the ability of the method to deal with non trivial geometrical changes.

I. Introduction

Sensitivity analysis has been the subject of active research for many years. It can be performed either by adjoint methods or by sensitivity equation approaches. In design optimization, adjoint techniques offer a clear advantage over sensitivity-based techniques when the number of parameters is large. However, adjoint variables only exist in an optimization context. On the other hand, sensitivities exist independently of any optimization problem and may be used for a variety of other applications including characterization of complex flows, parameter estimation, uncertainty analysis, fast evaluation of nearby flows, etc.^{1, 2, 3, 4}

Flow sensitivities can be obtained in two ways. In the approximate-then-differentiate approach (often called Discrete Sensitivity Equation (DSE) approach), the discrete form of the flow equations are differentiated and the total derivative of the flow discretization with respect to the design parameters is calculated. In the differentiate-then-approximate approach (known as the Continuous Sensitivity Equation method (CSE)), partial differential equations for the flow sensitivities are obtained by implicit differentiation of the equations governing the flow. They are then approximated numerically. The CSE method offers a number of advantages over discrete sensitivity algorithms that have been extensively discussed in the literature.^{5, 6}

Sensitivity analysis of turbulent flows have already been reported in the literature for value parameters.^{7, 8, 9, 1} However, treating shape parameters is more involved since the position of the boundaries of physical domains is parameter dependent. A major challenge arises when treating shape parameters since flow gradients appear as source terms in the CSE and as coefficients in their boundary conditions. Accurate spatial gradients in the interior of the computational domain can be obtained using an a posteriori gradient projection technique (which is already used for error estimation). However, this technique does not yield accurate derivatives on boundaries.¹⁰ A constrained Taylor series least-squares procedure on l -layered patches was proposed by Duvigneau and Pelletier⁶ to produce accurate boundary flow gradients. It has been shown that one must use at least 3rd order Taylor series on a 4-layer patch to achieve sufficient accuracy for the

*Graduate student

†Postdoctoral Fellow, AIAA Member

‡Research Fellow, AIAA Member

§Canada Research Chair, Associate Fellow AIAA

Dirichlet sensitivity boundary conditions and 4th order Taylor series on a 6-layer patch when Neumann conditions are imposed.⁶ Applications of the CSE method for shape parameters and laminar flows is reported in Ref. 4. In this paper, we extend the methodology to wall-bounded turbulent flows modeled with the standard $k - \epsilon$ turbulence model with wall functions based on two velocity scales. Thus, we have extended the constrained Taylor series least-squares procedure for handling wall functions sensitivity boundary conditions. We proceed in two steps. First, the reconstruction procedure is extended to the turbulence variables in the standard $k - \epsilon$ turbulence model. Second, the Taylor series least-squares procedure is modified to enforce constraints to ensure that the reconstructed solution fields satisfy the wall function boundary conditions.

The main difficulty in extending the SEM to wall-bounded turbulent flows, arises from the differentiation of wall functions to account for their complex shape parameter dependencies. The boundary condition for the flow in the tangential direction is prescribed as a function of the tangential velocity (mixed or Robin boundary condition). Differentiation of this boundary condition is not as straight forward as it appears in the case of a parameter dependent boundary. The methodology for dealing with such complex shape parameter dependencies is thoroughly described.

The paper is organized as follows. First, flow equations are presented in Section II and their associated boundary conditions in Section III. Section IV presents the Continuous Sensitivity Equations. In Section V, we details the shape sensitivity boundary conditions and the proper treatment of parameter dependent boundaries. Section VI introduces the finite-element formulation and the adaptive remeshing procedure based on the SUPG stabilization technique and the Taylor-Hood ($P_2 - P_1$) element. The proposed approach for computing both the flow and its sensitivities is then verified in Section VII on a problem with a closed-form solution derived using the Method of the Manufactured Solution.¹¹ Both the grid adaptive process and the finite-element solvers are verified simultaneously. We emphasize grid convergence of integrated forces along walls and of their gradients. Then, in Section VIII, the method is applied to turbulent flows around a square obstacle in proximity of a solid wall to investigate the ability of the CSE method to deal with non trivial geometrical changes and to predict important changes in the flow response.

II. Governing equations

The flows of interest are described by the Reynolds-Averaged Navier-Stokes (RANS) equations. The momentum and mass conservation laws are written as :

$$\rho \mathbf{u} \cdot \nabla \mathbf{u} = -\nabla p + \nabla \cdot \boldsymbol{\tau}(\mathbf{u}) + \mathbf{f} \quad (1)$$

$$\nabla \cdot \mathbf{u} = 0 \quad (2)$$

where ρ is the density, \mathbf{u} the velocity, p the pressure and \mathbf{f} the volumetric forces. Noting μ the molecular dynamic viscosity and μ_t the turbulent dynamic viscosity, the stress tensor $\boldsymbol{\tau}$ is defined according to the newton's law and the first order turbulence modelization approximation :

$$\boldsymbol{\tau}(\mathbf{u}) = (\mu + \mu_t) [\nabla \mathbf{u} + (\nabla \mathbf{u})^T]$$

The system is closed by computing the turbulent viscosity using the $k - \epsilon$ model. The eddy viscosity is computed from k and ϵ by :

$$\mu_t = \rho C_\mu \frac{k^2}{\epsilon} \quad (3)$$

To preserve positivity of the dependent variables, we work with the logarithmic form of these equations.¹² This can be viewed as using the following change of dependent variables :

$$\mathcal{K} = \ln(k) \quad \text{and} \quad \mathcal{E} = \ln(\epsilon) \quad (4)$$

The transport equations for the logarithmic variables are :

$$\begin{aligned} \rho \mathbf{u} \cdot \nabla \mathcal{K} &= \nabla \cdot \left[\left(\mu + \frac{\mu_t}{\sigma_k} \right) \nabla \mathcal{K} \right] + \left(\mu + \frac{\mu_t}{\sigma_k} \right) \nabla \mathcal{K} \cdot \nabla \mathcal{K} \\ &\quad + \mu_t e^{-\mathcal{K}} P - \rho^2 C_\mu \frac{e^\mathcal{K}}{\mu_t} + q_\mathcal{K} \end{aligned} \quad (5)$$

$$\begin{aligned} \rho \mathbf{u} \cdot \nabla \mathcal{E} &= \nabla \cdot \left[\left(\mu + \frac{\mu_t}{\sigma_\epsilon} \right) \nabla \mathcal{E} \right] + \left(\mu + \frac{\mu_t}{\sigma_\epsilon} \right) \nabla \mathcal{E} \cdot \nabla \mathcal{E} \\ &\quad + \rho C_1 C_\mu e^{\mathcal{K}-\mathcal{E}} P - C_2 \rho e^{\mathcal{E}-\mathcal{K}} + q_{\mathcal{E}} \end{aligned} \quad (6)$$

The production of turbulence P is defined as :

$$P = \nabla \mathbf{u} : [\nabla \mathbf{u} + (\nabla \mathbf{u})^T]$$

The constants appearing in these equations take on the standard values proposed by Launder and Spalding¹³ and are given in Table 1. Note that equations (5)-(6) are equivalent to the original equations of the turbulence

Table 1. Constant of the turbulence model

σ_k	σ_ϵ	$C_{\epsilon 1}$	$C_{\epsilon 2}$	C_μ
1.0	1.3	1.44	1.92	0.09

model; only the computational variables are different. Hence, the turbulence model is unchanged. The eddy viscosity is given by :

$$\mu_t = \rho C_\mu e^{2\mathcal{K}-\mathcal{E}} \quad (7)$$

III. Flow boundary conditions

This section focuses on the boundary conditions associated with the governing equations presented above. These equations are solved on a domain Ω with a boundary Γ .

A. Classical Dirichlet and Neumann boundary conditions

Boundaries of Ω that are not walls are modeled using standard Dirichlet and Neumann boundary conditions. They are imposed on boundaries Γ_D and Γ_N respectively :

- Dirichlet boundary conditions :

$$\mathbf{u} = \bar{\mathbf{u}} \quad ; \quad \mathcal{K} = \ln(\beta_k) \quad ; \quad \mathcal{E} = \ln(\beta_\epsilon) \quad (8)$$

- Neumann boundary conditions :

$$[-p\mathbf{I} + \tau(\mathbf{u})] \cdot \hat{\mathbf{n}} = \bar{\mathbf{t}} \quad ; \quad \left[\left(\mu + \frac{\mu_t}{\sigma_k} \right) \nabla \mathcal{K} \right] \cdot \hat{\mathbf{n}} = 0 \quad ; \quad \left[\left(\mu + \frac{\mu_t}{\sigma_\epsilon} \right) \nabla \mathcal{E} \right] \cdot \hat{\mathbf{n}} = 0 \quad (9)$$

where $\hat{\mathbf{n}}$ is an outward unit vector normal to the boundary, \mathbf{I} the second order identity tensor and β_k and β_ϵ small constants.

B. Wall boundary conditions

The standard $k - \epsilon$ turbulence model is not valid when the turbulent Reynolds number is low, as it is the case in near wall regions. Wall functions are used to describe the solution in these areas. For doing so, the computational wall boundary is taken at a distance d from the physical wall boundary. The gap between these two boundaries is the region where the flow is represented by the wall functions instead of being solved. In the remainder, the computational wall boundary will be referred to as the wall and quantities evaluated at it will be identified with the subscript w . We utilize the two-velocity scale wall functions described by Chabard¹⁴ and Ignat *et al*¹⁵ and presented in what follows.

A wall function expresses the value of u^+ , the non-dimensional velocity parallel to the solid wall, as a function of y^+ , the non-dimensional distance from the physical wall :

$$u^+ = \frac{1}{\kappa} \ln(Ey^+) \quad \text{for} \quad y^+ > 10.8 \quad (10)$$

where κ is the Karman constant and E a roughness parameter (for smooth walls we take $\kappa = 0.42$ and $E = 9.0$). The variables u^+ and y^+ are defined as follows :

$$y^+ = \frac{\rho du_k}{\mu} \quad \text{and} \quad u^+ = \frac{u_t}{u_{**}} \quad (11)$$

where $u_t = \mathbf{u} \cdot \hat{\mathbf{t}}$ denotes the tangential velocity, d is the normal distance to the physical wall and $u_{**} = \sqrt{\tau_w/\rho}$ the friction velocity. The specific value of d where the wall function is applied is chosen so that y^+ lies within the range of validity of the function (i.e. $30 < y^+ < 300$).¹⁶ A velocity scale based on the turbulence kinetic energy¹⁴ is computed by :

$$u_k = C_\mu^{\frac{1}{4}} k_w^{\frac{1}{2}} = C_\mu^{\frac{1}{4}} \exp\left(\frac{\mathcal{K}_w}{2}\right) \quad (12)$$

The boundary conditions associated to the governing equations are :

- flow boundary condition in the tangential direction : the constraint applied by the flow to the wall in the tangential direction is prescribed as a function of the tangential velocity (mixed or Robin boundary condition). Using the two-velocity scale wall function leads to a linear relationship between the shear stress at the wall τ_w in the direction of the flow and u_t .

$$[(\boldsymbol{\tau} \cdot \hat{\mathbf{n}}) \cdot \hat{\mathbf{t}}]_{wall} = \tau_w = \rho u_k u_{**} = \frac{\rho u_k}{\frac{1}{\kappa} \ln(E \frac{\rho du_k}{\mu})} u_t \quad (13)$$

- flow boundary condition in the normal direction : the normal velocity is set to zero.

$$\mathbf{u} \cdot \hat{\mathbf{n}} = 0 \quad (14)$$

- boundary condition for \mathcal{K} : The \mathcal{K} -equation is solved with a zero auxiliary flux boundary condition. This condition arises from the fact that the wall shear stress is considered constant in the wall functions region (i.e. $0 < y^+ < 300$).¹⁶ This Neumann condition is required to compute the distribution of u_k along the wall.

$$\left(\mu + \frac{\mu_t}{\sigma_k}\right) \nabla \mathcal{K} \cdot \hat{\mathbf{n}} = 0 \quad (15)$$

- boundary condition for \mathcal{E} : The boundary condition for the logarithm of ϵ is the logarithm of the usual Dirichlet boundary condition for the turbulence kinetic energy dissipation rate at walls but the velocity scaled u_k is used instead of u_{**} .

$$\mathcal{E} = \ln\left(\frac{u_k^3}{\kappa d}\right) \quad (16)$$

IV. Continuous Sensitivity Equations

The Continuous Sensitivity Equations are derived formally by direct differentiation of the flow equations (Eqs. (1)-(2)) and the turbulence variables equations (Eqs. (5)-(6)) with respect to an arbitrary parameter a . Thus, we treat any variable \mathbf{u} as a function of both space and parameter a . This dependency is denoted by $\mathbf{u} = \mathbf{u}(\mathbf{x}; a)$. The sensitivities are defined as the partial derivatives :

$$\mathbf{s}_{\mathbf{u}} = \frac{\partial \mathbf{u}}{\partial a} \quad ; \quad s_p = \frac{\partial p}{\partial a} \quad ; \quad s_{\mathcal{K}} = \frac{\partial \mathcal{K}}{\partial a} \quad ; \quad s_{\mathcal{E}} = \frac{\partial \mathcal{E}}{\partial a} \quad (17)$$

Then, CSE governing sensitivity fields are written as :

$$\rho' \mathbf{u} \cdot \nabla \mathbf{u} + \rho (\mathbf{s}_u \cdot \nabla \mathbf{u} + \mathbf{u} \cdot \nabla \mathbf{s}_u) = -\nabla s_p + \nabla \cdot \tau(\mathbf{s}_u) + \nabla \cdot \tau'(\mathbf{u}) + \mathbf{f}_s \quad (18)$$

$$\nabla \cdot \mathbf{s}_u = 0 \quad (19)$$

$$\begin{aligned} \rho' \mathbf{u} \cdot \nabla \mathcal{K} + \rho (\mathbf{s}_u \cdot \nabla \mathcal{K} + \mathbf{u} \cdot \nabla s_{\mathcal{K}}) &= \nabla \cdot \left[\left(\mu' + \frac{\mu'_t}{\sigma_k} - \frac{\mu_t \sigma'_k}{\sigma_k^2} \right) \nabla \mathcal{K} + \left(\mu + \frac{\mu_t}{\sigma_k} \right) \nabla s_{\mathcal{K}} \right] \\ &+ \left(\mu' + \frac{\mu'_t}{\sigma_k} - \frac{\mu_t \sigma'_k}{\sigma_k^2} \right) \nabla \mathcal{K} \cdot \nabla \mathcal{K} \quad (20) \\ &+ 2 \left(\mu + \frac{\mu_t}{\sigma_k} \right) \nabla \mathcal{K} \cdot \nabla S_{\mathcal{K}} + e^{-\mathcal{K}} (\mu'_t P + \mu_t P' - \mu_t P s_{\mathcal{K}}) \\ &- \rho e^{\mathcal{E}-\mathcal{K}} \left(2 \frac{\rho'}{\rho} + \frac{C'_\mu}{C_\mu} + s_{\mathcal{K}} - \frac{\mu'_t}{\mu_t} \right) \end{aligned}$$

$$\begin{aligned} \rho' \mathbf{u} \cdot \nabla \mathcal{E} + \rho (\mathbf{s}_u \cdot \nabla \mathcal{E} + \mathbf{u} \cdot \nabla s_{\mathcal{E}}) &= \nabla \cdot \left[\left(\mu' + \frac{\mu'_t}{\sigma_\epsilon} - \frac{\mu_t \sigma'_\epsilon}{\sigma_\epsilon^2} \right) \nabla \mathcal{E} + \left(\mu + \frac{\mu_t}{\sigma_\epsilon} \right) \nabla s_{\mathcal{E}} \right] \\ &+ \left(\mu' + \frac{\mu'_t}{\sigma_\epsilon} - \frac{\mu_t \sigma'_\epsilon}{\sigma_\epsilon^2} \right) \nabla \mathcal{E} \cdot \nabla \mathcal{E} + 2 \left(\mu + \frac{\mu_t}{\sigma_\epsilon} \right) \nabla \mathcal{E} \cdot \nabla S_{\mathcal{E}} \quad (21) \\ &+ \rho C_{\epsilon 1} C_\mu e^{\mathcal{K}-\mathcal{E}} P \left(\frac{\rho'}{\rho} + \frac{C'_{\epsilon 1}}{C_{\epsilon 1}} + \frac{C'_\mu}{C_\mu} + S_{\mathcal{K}} - S_{\mathcal{E}} + \frac{P'}{P} \right) \\ &- C_{\epsilon 2} \rho e^{\mathcal{E}-\mathcal{K}} \left(\frac{C'_{\epsilon 2}}{C_{\epsilon 2}} + \frac{\rho'}{\rho} + S_{\mathcal{E}} - S_{\mathcal{K}} \right) \end{aligned}$$

the partial derivatives of the fluid properties being denoted using a ('), \mathbf{f}_s being the sensitivity of the volumetric forces and having :

$$\begin{aligned} \tau'(\mathbf{u}) &= (\mu' + \mu'_t) [\nabla \mathbf{u} + (\nabla \mathbf{u})^T] \\ \tau(\mathbf{s}_u) &= (\mu + \mu_t) [\nabla \mathbf{s}_u + (\nabla \mathbf{s}_u)^T] \\ P' &= 2 \nabla \mathbf{s}_u : [\nabla \mathbf{u} + (\nabla \mathbf{u})^T] \end{aligned}$$

with the sensitivity of the eddy-viscosity given by :

$$\mu'_t = \mu_t \left(\frac{\rho'}{\rho} + \frac{C'_\mu}{C_\mu} + 2s_{\mathcal{K}} - s_{\mathcal{E}} \right) \quad (22)$$

Finally, the sensitivities of the turbulence variables and those of their logarithms are related through :

$$S_{\mathcal{K}} = \frac{S_k}{k} \quad ; \quad S_{\mathcal{E}} = \frac{S_\epsilon}{\epsilon} \quad (23)$$

V. Shape sensitivity boundary conditions

To complete the description of the sensitivity problem, the boundary conditions presented in section III are differentiated in the same way. However, if a is a shape parameter, the position of the boundary is parameter dependent. Thus, the differentiation should account for the fact that both the boundary location and the boundary condition both depend on a . Furthermore, boundary conditions arise from physical modeling. Thus, they can be applied only on physical boundaries. As a consequence, differentiation of these conditions must be performed while following the boundaries through their deformations. In other words, the material derivatives have to be considered.

For doing so, the parameter dependent boundaries have to be properly described. Some geometrical issues linked to shape parameters are thus first addressed in the next subsection before presenting the differentiation of the flow boundary conditions.

A. Describing parameter dependent boundaries

For shape parameter, the points on the boundary Γ of the computational domain depend on the parameter a of interest. The parameter dependent boundary Γ is parameterized by ξ , the curvilinear coordinate of a

point on Γ (the arc length is often used). Parameter a determines the shape of Γ while ξ determines the location of a point on Γ . Therefore, any point $\hat{\mathbf{X}}$ of the boundary surface depends both on a and ξ :

$$\Gamma(a) = \{ \hat{\mathbf{X}}(\xi, a) \mid \xi \in [\xi_0, \xi_1] \} \quad (24)$$

For this parameterized boundary, the unit normal vectors $\hat{\mathbf{n}}(\xi, a)$ and the unit tangent vector $\hat{\mathbf{t}}(\xi, a)$ can be expressed in terms of the derivatives of $\hat{\mathbf{X}}$ with respect to ξ . Any change to a will affect all these

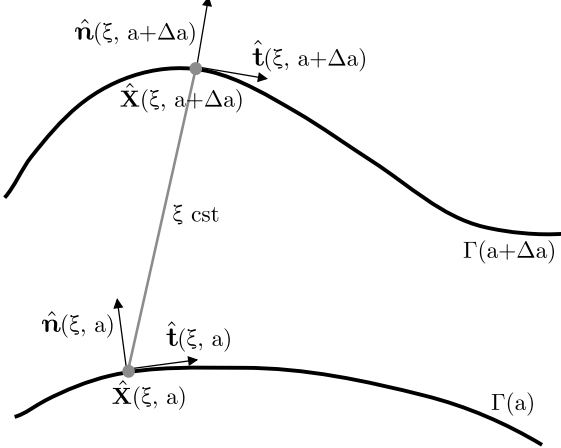


Figure 1. Notations relative to boundary surface

geometrical quantities. Note that, their material derivatives reduce to their partial derivatives if one uses the curve description Eq. (24). This apparently burdensome notation is the key to successful differentiation of geometrical quantities appearing in sensitivity boundary conditions. Note that, if one follows a given point on Γ , ξ remains constant as a varies to change the shape of Γ as illustrated in Figure 1. This leads to the following relations :

$$\begin{aligned} \frac{D\hat{\mathbf{X}}}{Da}(\xi, a) &= \frac{\partial \hat{\mathbf{X}}}{\partial a}(\xi, a) \\ \frac{D\hat{\mathbf{n}}}{Da}(\xi, a) &= \frac{\partial \hat{\mathbf{n}}}{\partial a}(\xi, a) \\ \frac{D\hat{\mathbf{t}}}{Da}(\xi, a) &= \frac{\partial \hat{\mathbf{t}}}{\partial a}(\xi, a) \end{aligned}$$

where D/Da denote the material derivative with respect to a .

Let $\phi(\hat{\mathbf{X}}(\xi, a), a)$ be any solution variable or physical property evaluated at a boundary. Using the chain rule, its material derivative can be expressed as the sum of its sensitivity (i.e. its partial derivative) and a transpiration term accounting for the modification of the shape of the boundary :

$$\frac{D\phi}{Da}(\hat{\mathbf{X}}(\xi, a), a) = \frac{\partial \phi}{\partial a} + \nabla \phi \cdot \frac{\partial \hat{\mathbf{X}}}{\partial a} \rightarrow \frac{\partial \phi}{\partial a} = \frac{\mathbf{D}\phi}{\mathbf{D}\mathbf{a}} - \nabla \phi \cdot \frac{\partial \hat{\mathbf{X}}}{\partial \mathbf{a}} \quad (25)$$

B. Classical Dirichlet and Neumann boundary conditions

We first present the derivation of the classical Dirichlet and Neumann boundary conditions (Eqs. (8) and (9)). As explained previously, only the material derivatives of these conditions are known. However, sensitivity boundary conditions are derived from them and relation (25). Doing so, the following boundary conditions are obtained.

- Dirichlet boundary condition on Γ_D :

$$\begin{aligned}\mathbf{s}_{\mathbf{u}} &= \frac{D\bar{\mathbf{u}}}{Da} - \nabla \mathbf{u} \cdot \frac{\partial \hat{\mathbf{X}}}{\partial a} \\ s_{\mathcal{K}} &= \frac{\beta'_k}{\beta_k} - \nabla \mathcal{K} \cdot \frac{\partial \hat{\mathbf{X}}}{\partial a} \\ s_{\mathcal{E}} &= \frac{\beta'_{\epsilon}}{\beta_{\epsilon}} - \nabla \mathcal{E} \cdot \frac{\partial \hat{\mathbf{X}}}{\partial a}\end{aligned}\quad (26)$$

- Neumann boundary condition on Γ_N :

$$\begin{aligned}[-s_p \mathbf{I} + \tau'(\mathbf{u}) + \tau(\mathbf{s}_{\mathbf{u}})] \cdot \hat{\mathbf{n}} &= \frac{D\bar{\mathbf{t}}}{Da} - \left[\nabla [-p\mathbf{I} + \tau(\mathbf{u})] \cdot \frac{\partial \hat{\mathbf{X}}}{\partial a} \right] \cdot \hat{\mathbf{n}} \\ &\quad - [-p\mathbf{I} + \tau(\mathbf{u})] \cdot \frac{\partial \hat{\mathbf{n}}}{\partial a} \\ \left[\left(\mu' + \frac{\mu'_t}{\sigma_k} - \frac{\mu_t \sigma'_k}{\sigma_k^2} \right) \nabla \mathcal{K} + \left(\mu + \frac{\mu_t}{\sigma_k} \right) \nabla s_{\mathcal{K}} \right] \cdot \hat{\mathbf{n}} &= - \left[\nabla \mu \cdot \frac{\partial \hat{\mathbf{X}}}{\partial a} + \frac{\nabla \mu_t \cdot \frac{\partial \hat{\mathbf{X}}}{\partial a}}{\sigma_k} \right] \nabla \mathcal{K} \cdot \hat{\mathbf{n}} \\ &\quad - \left(\mu + \frac{\mu_t}{\sigma_k} \right) \left[\nabla \mathcal{K} \cdot \frac{\partial \hat{\mathbf{n}}}{\partial a} + \nabla (\nabla \mathcal{K}) \cdot \frac{\partial \hat{\mathbf{X}}}{\partial a} \cdot \hat{\mathbf{n}} \right] \\ \left[\left(\mu' + \frac{\mu'_t}{\sigma_{\epsilon}} - \frac{\mu_t \sigma'_{\epsilon}}{\sigma_{\epsilon}^2} \right) \nabla \mathcal{E} + \left(\mu + \frac{\mu_t}{\sigma_{\epsilon}} \right) \nabla s_{\mathcal{E}} \right] \cdot \hat{\mathbf{n}} &= - \left[\nabla \mu \cdot \frac{\partial \hat{\mathbf{X}}}{\partial a} + \frac{\nabla \mu_t \cdot \frac{\partial \hat{\mathbf{X}}}{\partial a}}{\sigma_{\epsilon}} \right] \nabla \mathcal{E} \cdot \hat{\mathbf{n}} \\ &\quad - \left(\mu + \frac{\mu_t}{\sigma_{\epsilon}} \right) \left[\nabla \mathcal{E} \cdot \frac{\partial \hat{\mathbf{n}}}{\partial a} + \nabla (\nabla \mathcal{E}) \cdot \frac{\partial \hat{\mathbf{X}}}{\partial a} \cdot \hat{\mathbf{n}} \right]\end{aligned}\quad (27)$$

As can be seen, for a shape parameter, the first derivatives of the flow and turbulence variables are needed to evaluate Dirichlet boundary conditions and second derivatives are required for evaluating Neumann boundary conditions. This introduces numerical difficulties when solving the CSE, since approximate boundary conditions are used. In practice, boundary conditions are evaluated using high order Taylor series expansions on layered patches in conjunction with a constrained least-square procedure.⁶

C. Wall boundary conditions for sensitivities

The differentiation of the wall boundary conditions presented in section III leads to the following boundary conditions for CSE.

- flow sensitivity boundary condition in the tangential direction :

$$\begin{aligned}\left[\left(\frac{\partial \tau}{\partial a} \cdot \hat{\mathbf{n}} \right) \cdot \hat{\mathbf{t}} \right]_{wall} &= \left(\rho' + \nabla \rho \cdot \frac{\partial \hat{\mathbf{X}}}{\partial a} \right) u_k u_{**} \\ &\quad + \rho u_k \frac{Du_{**}}{Da} + \rho u_{**} \frac{Du_k}{Da} - \tau \cdot \frac{\partial \hat{\mathbf{n}}}{\partial a} \cdot \hat{\mathbf{t}} \\ &\quad - \tau \cdot \hat{\mathbf{n}} \cdot \frac{\partial \hat{\mathbf{t}}}{\partial a} - \left[\left(\nabla \tau \cdot \frac{\partial \hat{\mathbf{X}}}{\partial a} \right) \cdot \hat{\mathbf{n}} \right] \cdot \hat{\mathbf{t}}\end{aligned}\quad (28)$$

with the material derivatives of the velocity scales given by :

$$\frac{Du_k}{Da} = u_k \left[\frac{C'_\mu}{4C_\mu} + \frac{1}{2k_w} \left(s_k + \nabla k \cdot \frac{\partial \hat{\mathbf{X}}}{\partial a} \right) \right] = u_k \left[\frac{C'_\mu}{4C_\mu} + \frac{1}{2} \left(s_{\mathcal{K}} + \nabla \mathcal{K} \cdot \frac{\partial \hat{\mathbf{X}}}{\partial a} \right) \right] \quad (29)$$

$$\begin{aligned} \frac{Du_{**}}{Da} &= \frac{\kappa}{\ln(\frac{E\rho du_k}{\mu})} \left\{ \frac{\kappa' u_t}{\kappa} + \left(\mathbf{s}_u + \nabla \mathbf{u} \cdot \frac{\partial \hat{\mathbf{X}}}{\partial a} \right) \cdot \hat{\mathbf{t}} + \mathbf{u} \cdot \frac{\partial \hat{\mathbf{t}}}{\partial a} \right. \\ &\quad \left. - \frac{u_t}{\ln(\frac{E\rho du_k}{\mu})} \left[\frac{E'}{E} + \frac{d'}{d} + \frac{1}{u_k} \frac{Du_k}{Da} + \frac{\left(\rho' + \nabla \rho \cdot \frac{\partial \hat{\mathbf{X}}}{\partial a} \right)}{\rho} - \frac{\left(\mu' + \nabla \mu \cdot \frac{\partial \hat{\mathbf{X}}}{\partial a} \right)}{\mu} \right] \right\} \end{aligned} \quad (30)$$

Note that (28) is a mixed boundary condition since $\left(\frac{\partial \tau}{\partial a} \cdot \hat{\mathbf{n}} \right) \cdot \hat{\mathbf{t}}$ is related to $\mathbf{s}_u \cdot \hat{\mathbf{t}}$ through $\frac{Du_{**}}{Da}$.

Note also that Eqs. (28) and (30) can be simplified in the particular case of incompressible flow since the spatial gradient of the density is always zero.

- flow sensitivity boundary condition in the normal direction :

$$\mathbf{s}_u \cdot \hat{\mathbf{n}} = - \left(\nabla \mathbf{u} \cdot \frac{\partial \hat{\mathbf{X}}}{\partial a} \right) \cdot \hat{\mathbf{n}} - \mathbf{u} \cdot \frac{\partial \hat{\mathbf{n}}}{\partial a} \quad (31)$$

- boundary condition for $s_{\mathcal{K}}$:

$$\begin{aligned} \left[\left(\mu' + \frac{\mu'_t}{\sigma_k} - \frac{\mu_t \sigma'_k}{\sigma_k^2} \right) \nabla \mathcal{K} + \left(\mu + \frac{\mu_t}{\sigma_k} \right) \nabla s_{\mathcal{K}} \right] \cdot \hat{\mathbf{n}} &= - \left[\nabla \mu \cdot \frac{\partial \hat{\mathbf{X}}}{\partial a} + \frac{\nabla \mu_t \cdot \frac{\partial \hat{\mathbf{X}}}{\partial a}}{\sigma_k} \right] \nabla \mathcal{K} \cdot \hat{\mathbf{n}} \\ &\quad - \left(\mu + \frac{\mu_t}{\sigma_k} \right) \left[\nabla \mathcal{K} \cdot \frac{\partial \hat{\mathbf{n}}}{\partial a} + \nabla (\nabla \mathcal{K}) \cdot \frac{\partial \hat{\mathbf{X}}}{\partial a} \cdot \hat{\mathbf{n}} \right] \end{aligned} \quad (32)$$

- boundary condition for $s_{\mathcal{E}}$:

$$s_{\mathcal{E}} = \frac{3}{u_k} \frac{Du_k}{Da} - \frac{\kappa'}{\kappa} - \frac{d'}{d} - \nabla \mathcal{E} \cdot \frac{\partial \hat{\mathbf{X}}}{\partial a} \quad (33)$$

VI. Finite element formulation and adaptive remeshing

The RANS equations and the logarithmic form of the turbulence equations are solved by a finite element method. The velocity and the logarithmic turbulence variables are discretized using 6-noded quadratic elements. Fluid pressure is discretized by piecewise linear continuous functions (element $P_2 - P_1$). For high Reynolds number, the equations are dominated by convection so that the standard Galerkin discretization may lead to non-physical oscillations and convergence difficulties. Hence, some form of upwinding is required. This is done by using the Streamline Upwind/Petrov-Galerkin (SUPG) stabilized formulation initially proposed by Brooks and Hughes¹⁷ and further improved by Ilinca *et al.*¹⁸ The discretization of the equations leads to a system of non-linear algebraic equations which are linearized by Newton's method. All linear algebraic systems are solved using a skyline direct solver.

Mesh independent solutions of the equations are obtained with an adaptive finite element algorithm.¹⁹ Error estimates are obtained by a local least-squares reconstruction of the solution derivatives for the velocity field and the logarithms of turbulence variables. An error estimate for the eddy viscosity is also constructed since slowly varying fields of \mathcal{K} and \mathcal{E} may result in rapid variation of μ_t . Finally, a reconstruction error estimate for the pressure is also computed. The adaptive methodology is set to reduce the error on each variable by a factor of two at each cycle of adaptation.

VII. Verification by the Method of the Manufactured Solution

A. Definition of the problem

The manufactured solution mimics the near-wall behavior of a two-dimensional, steady incompressible turbulent boundary-layer. The near-wall behavior of all the specified quantities is similar to what is observed in near-wall turbulent flows and the Reynolds number is set to one million. The manufactured solution and the source terms defining the modified problem are thoroughly described in Ref. 20. Additional source terms are required to verify wall functions; see details in Ref. 21. Thus, we extend the manufactured solution to verify wall functions for sensitivity analysis of shape parameters. We focus on sensitivity of the flow response with respect to the vertical position of the flat wall along which the turbulent boundary-layer is developing. The problem is illustrated in Figure 2 where y_0 is the shape parameter for the sensitivity analysis. For completeness, we briefly describe the manufactured flow and sensitivity fields. As illustrated

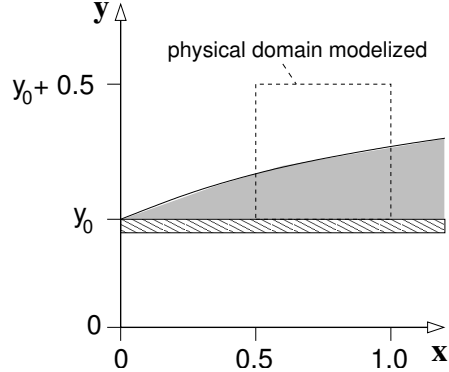


Figure 2. Manufactured problem: computational domain

in Figure 2, the physical domain is a square of side $0.5L$ with $0.5L \leq x \leq L$ and $0 \leq y - y_0 \leq 0.5L$. The Reynolds number Re is defined by $Re = \frac{U_1 L}{\nu}$ where U_1 is the reference velocity, L the reference length and ν the kinematic viscosity. All quantities presented below are non-dimensional using L and U_1 as the reference length and velocity scale.

In the definition of the velocity components and pressure coefficient we will use the following *similarity variable* with $\sigma = 4$. and $\sigma_\nu = 2.5\sigma$:

$$\eta = \frac{\sigma(y - y_0)}{x} ; \quad \eta_\nu = \frac{\sigma_\nu(y - y_0)}{x} \quad (34)$$

The velocity component in the x direction, u , is given by

$$u = \text{erf}(\eta) \quad (35)$$

The velocity component in the y direction, v , is given by

$$v = \frac{1}{\sigma\sqrt{\pi}} \left(1 - e^{-\eta^2} \right) \quad (36)$$

and the pressure is given by :

$$p = 0.5 \ln(2x - x^2 + 0.25) \ln(4y^3 - 3y^2 + 1.25) \quad (37)$$

The field of k for the MS is generated using the following equation with $k_{max} = 0.01$:

$$k = k_{max} \eta_\nu^2 e^{1-\eta_\nu^2} + \alpha_k \quad (38)$$

The dissipation rate ϵ is as follows with $\nu_{max} = 0.001$:

$$\epsilon = 0.36 \frac{k_{max}^2}{\nu_{max}} e^{-\eta_\nu^2} + \alpha_\epsilon \quad (39)$$

Finally, the eddy-viscosity is obtained from

$$\nu_t = c_\mu \frac{k^2}{\epsilon} \quad (40)$$

We have added small constants α_k and α_ϵ to the MS Fields for k and ϵ described in Ref. 20 to avoid logarithms of zero values. Recall that the computational variables for the turbulence model are the logarithms of k and ϵ . See Ref. 22 for details.

$$\alpha_k = 10^{-5} \quad ; \quad \alpha_\epsilon = 10^{-3} \quad (41)$$

The analytical solution for all variables is imposed on the inflow and upper boundaries as Dirichlet boundary conditions. On the outlet, the normal and tangential forces on the boundary are imposed from the exact velocity and pressure fields. The diffusion fluxes of k and ϵ are also imposed from the exact solution. Hence, on the outlet Neumann boundary conditions are applied on all variables. On the wall (bottom boundary), the type of boundary conditions is set in accordance with those employed for using wall functions (see Section B) :

- u : Robin boundary condition
- v : Dirichlet boundary condition
- k : Neumann boundary condition
- ϵ : Dirichlet boundary condition

As described in Ref. 21, source terms are added in the classical wall functions boundary conditions to fit with the manufactured solution. The wall distance is set to $d = 0.006$ which ensures, for a Reynolds number of one million, that the non-dimensional wall distance (Eq. 11) lies in [30, 300] on all the wall while being as close as possible of the lower limit.

Direct differentiation with respect to y_0 yields the following expressions for the sensitivities of the flow and turbulent :

$$\begin{aligned} S_u &= -\frac{2\sigma}{x\sqrt{\pi}} e^{-\eta^2} \\ S_v &= -\frac{2\eta}{x\sqrt{\pi}} e^{-\eta^2} \\ S_p &= \frac{3(y-y_0)[1-2(y-y_0)]}{4(y-y_0)^3 - 3(y-y_0)^2 + 1.25} \log(2x - x^2 + 0.25) \\ S_k &= \frac{2k_{max}\sigma_\nu}{x} \eta_\nu (\eta_\nu^2 - 1) e^{(1-\eta_\nu^2)} \\ S_\epsilon &= \frac{0.72k_{max}^2\sigma_\nu}{x\nu_{max}} \eta_\nu e^{-\eta_\nu^2} \end{aligned}$$

The boundary conditions for the sensitivity problem are deduced from the flow boundary conditions described above (see Section C for more details).

B. Verification of flow and sensitivity

The flow and sensitivity fields are solved using the adaptive finite-element method. On parameter dependent boundary curves, boundary conditions for the sensitivity problem are computed using the constrained 6th order Taylor series least-squares reconstruction of flow variables on 8-layered patches.⁶ This ensures a sufficiently accurate evaluation of transpiration terms in the sensitivity boundary conditions. All flow and sensitivity variables contribute to the error estimation so that the mesh adaptation process is driven by 10 error estimates (velocity, pressure, k , ϵ and μ_t and their corresponding sensitivities). Eight grid adaptation cycles have been performed. Figure 3 shows the final mesh containing 123 689 nodes. It is typical of adapted meshes for boundary layer flow problems as expected. Extensive refinement is observed in the near-wall region. Several bands of refinement can also be identified which correspond to regions of rapid variation in velocity, \mathcal{K} , \mathcal{E} and μ_t and their sensitivities.

Figure 4 presents the trajectories of true and estimated error norms for the flow variables and their

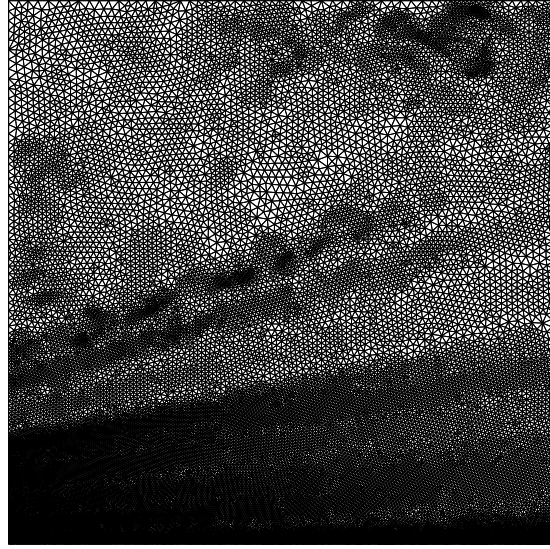


Figure 3. Manufactured solution : Final adapted mesh

sensitivities. The norms showed are the following :

$$\begin{aligned}
 \text{H1U} &: \|u\|_{H^1} = \sqrt{\int_{\Omega} (\nabla u \cdot \nabla u + \nabla v \cdot \nabla v) d\Omega} \\
 \text{H1P} &: \|p\|_{H^1} = \sqrt{\int_{\Omega} \nabla p \cdot \nabla p d\Omega} \\
 \text{EVM} &: \|\mu_t\|_{eqv} = \sqrt{\int_{\Omega} \nabla \mu_t \cdot \nabla \mu_t d\Omega}
 \end{aligned}$$

As can be seen, errors on both the flow and the sensitivities decrease from cycle to cycle. The trajectory of the error estimators converges to that of the true error with mesh adaption. This property (asymptotic exactness) implies that the error estimators become more accurate and reliable with mesh refinement.

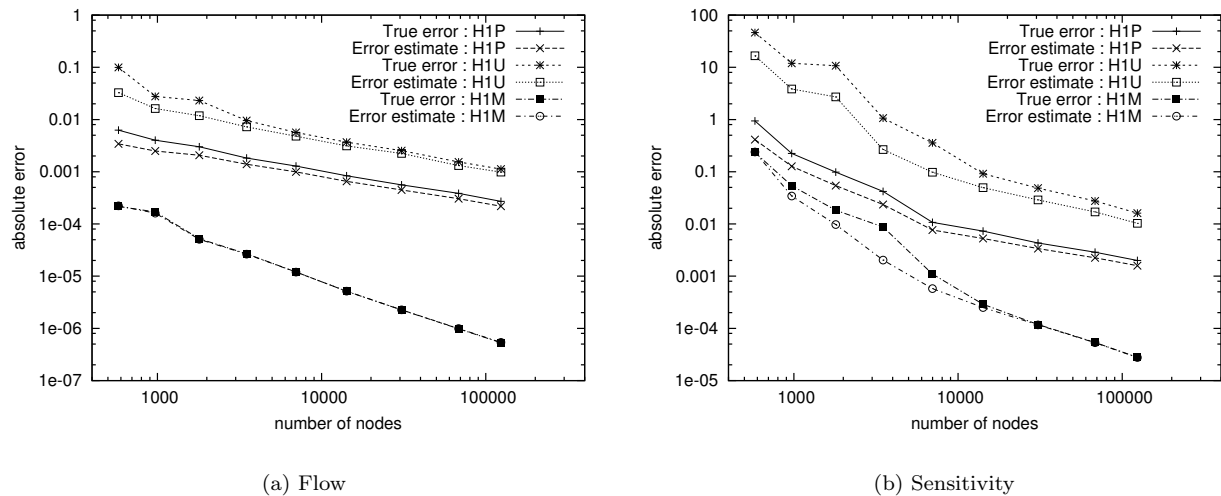


Figure 4. Manufactured solution : Trajectories of true and estimated error norms

We now turn our attention to the evaluation the friction resistance R_f on the wall and its sensitivity, two integral quantities. Taking $\rho U_{\text{ref}}^2 L_{\text{ref}}$ as a reference force, the friction resistance is computed as follows :

$$R_f = \frac{1}{\rho U_{\text{ref}}^2 L_{\text{ref}}} \int_{\Gamma_w} \tau \cdot \hat{\mathbf{n}} \cdot \hat{\mathbf{t}} \, d\Gamma = \int_{\Gamma_w} \left[(\mu + \mu_t) \left(\frac{\partial u}{\partial y} + \frac{\partial v}{\partial x} \right) \right] \, d\Gamma$$

The last integral is a simplified expression for our particular case with $\hat{\mathbf{n}} = [0, 1]^T; \hat{\mathbf{t}} = [1, 0]^T$.

Direct differentiation of the above expression yields the sensitivity of the friction coefficient which is an Eulerian derivative in the parameter space. Using the following derivatives of the geometric quantities :

$$\frac{\partial \hat{\mathbf{n}}}{\partial y_0} = \frac{\partial \hat{\mathbf{t}}}{\partial y_0} = [0, 0]^T \quad ; \quad \frac{\partial \hat{X}}{\partial y_0} = [0, 1]^T \quad (42)$$

leads to the following simplified expression for the Eulerian sensitivity of the friction resistance :

$$\frac{\partial R_f}{\partial y_0} = \int_{\Gamma_w} \left[(\mu + \mu_t) \left(\frac{\partial S_u}{\partial y} + \frac{\partial S_v}{\partial x} \right) + S_{\mu_t} \left(\frac{\partial u}{\partial y} + \frac{\partial v}{\partial x} \right) \right] \, d\Gamma \quad (43)$$

The required Lagrangian sensitivity is easily derived using the material derivative in parameter space. The expression can be simplified for our particular case :

$$\begin{aligned} \frac{dR_f}{dy_0} &= \frac{1}{\rho U_{\text{ref}}^2 L_{\text{ref}}} \int_{\Gamma_w} \frac{d\tau}{dy_0} \cdot \hat{\mathbf{n}} \cdot \hat{\mathbf{t}} \, d\Gamma \\ &= \frac{1}{\rho U_{\text{ref}}^2 L_{\text{ref}}} \int_{\Gamma_w} \left(\frac{\partial \tau}{\partial y_0} + \nabla \tau \cdot \frac{\partial \hat{X}}{\partial y_0} \right) \cdot \hat{\mathbf{n}} \cdot \hat{\mathbf{t}} \, d\Gamma \\ &= \frac{\partial R_f}{\partial y_0} + \frac{1}{\rho U_{\text{ref}}^2 L_{\text{ref}}} \int_{\Gamma_w} \nabla \tau \cdot \frac{\partial \hat{X}}{\partial y_0} \cdot \hat{\mathbf{n}} \cdot \hat{\mathbf{t}} \, d\Gamma \\ &= \frac{\partial R_f}{\partial y_0} + \frac{1}{\rho U_{\text{ref}}^2 L_{\text{ref}}} \int_{\Gamma_w} [(\mu + \mu_t) \left(\frac{\partial^2 u}{\partial y^2} + \frac{\partial^2 v}{\partial x^2} \right) + S_{\mu_t} \left(\frac{\partial u}{\partial y} + \frac{\partial v}{\partial x} \right)] \, d\Gamma \end{aligned} \quad (44)$$

As can be seen, the Lagrangian sensitivity is equal to the Eulerian sensitivity plus a transpiration term (last term of the third and fourth lines) which accounts for the change in the position of the wall boundary caused by changes in the parameter y_0 . Since the wall boundary condition does not depend on y_0 , its Lagrangian derivative is zero. This is confirmed by Table 2 which gives the exact value of the Friction Coefficient and its sensitivities. This means that the transpiration term (last term of the fourth line in Eq. 44) exactly cancels out the Eulerian sensitivity given by Eq. 43. This can easily be seen since $\frac{\partial \tau}{\partial y} = -\frac{\partial \cdot}{\partial y_0}$.

Figure 5 shows the evolution of the exact errors in R_f and its sensitivities with adaptive cycles. As can

Exact Friction Coefficient	Exact Eulerian sensitivity	Exact Lagrangian sensitivity
$R_f = 0.354686 \cdot 10^{-5}$	$\frac{\partial R_f}{\partial y_0} = -0.267451 \cdot 10^{-3}$	$\frac{dR_f}{dy_0} = 0$

Table 2. Manufactured solution : Friction resistance

be seen, the errors decrease from cycle to cycle. Hence, the errors on the gradient of integral forces can be reduced as much as desired using the adaptive process. The proposed methodology for computing the gradient of integral forces is thus verified as well as the expressions for the transpiration terms.

We now briefly illustrate how sensitivity information can be used for evaluation of solution on nearby geometries. First order Taylor series expansion of the flow response in the parameter space are used for this purpose. We consider a change of $\Delta y_0 = 0.02$ in the shape parameter from its baseline value of zero. We compare the baseline flow, the first order extrapolation from $y_0 = 0$ to $y_0 = 0.02$ and the recomputed flow at $y_0 = 0.04$ (reanalysis). Figure 6 shows the contours of the horizontal velocity and Figure 7 those of the pressure. As can be seen, the agreement between reanalysis and extrapolation results are almost perfect. This shows first that the numerical evaluation of the flow sensitivities is accurate. Second, it tells us that the change in the shape parameter is sufficiently small to ensure that the linear Taylor series in parameter space is a reliable approximation of the flow variable dependence on y_0 , in spite of the apparently complicated relationships given by Eqs (35)-(40).

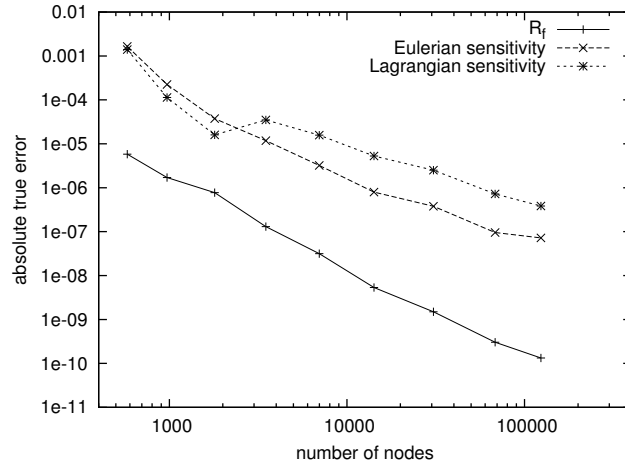


Figure 5. Grid convergence of the sensitivities of the friction resistance on the wall

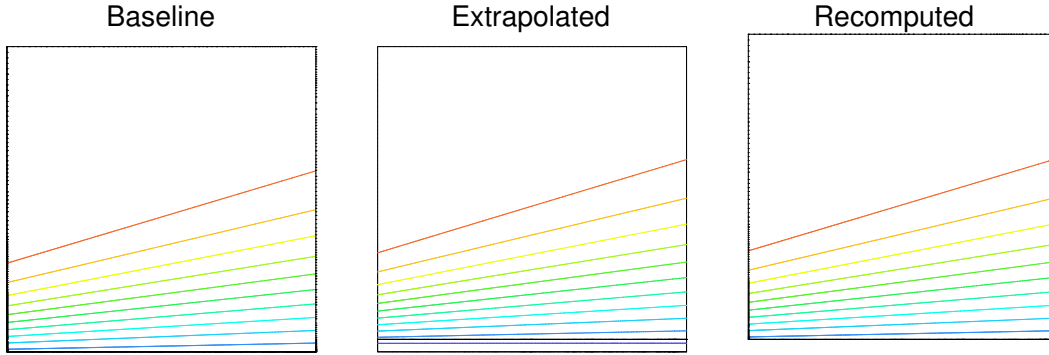


Figure 6. Baseline, extrapolated and recomputed isolines of the horizontal velocity

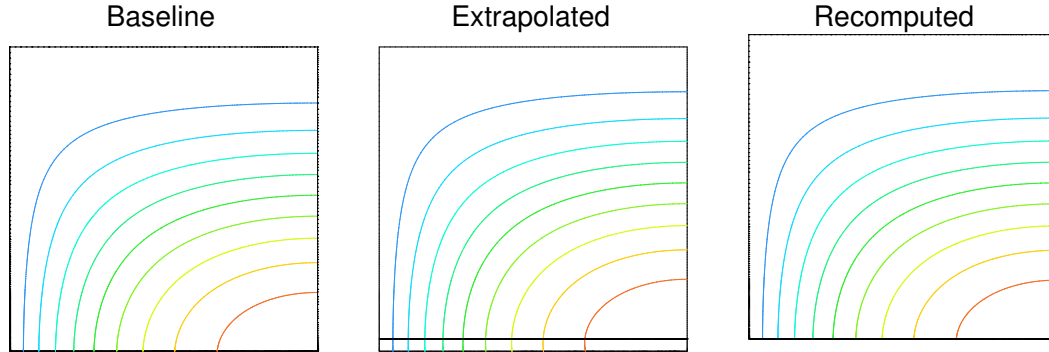


Figure 7. Baseline, extrapolated and recomputed iso-lines of the pressure

VIII. Application to turbulent flow around a square obstacle

A. Definition of the problem

We consider the flow of air around a square cross-section cylinder in the proximity of a solid wall as investigated by Wu and Martinuzzi using Laser Doppler Velocimetry.²³ The experimental configuration consists of a smooth flat plate located in the $0.45 \text{ m} \times 0.45 \text{ m}$ test section of a suction-type wind tunnel. Details of the experimental set-up are shown in Fig. 8. Experiments were conducted for a Reynolds number of 22,000,

based on D , the dimension of the side of the square obstacle U_0 , the inlet velocity. The oncoming free stream turbulence intensity is set at 1% and the mean flow is steady.

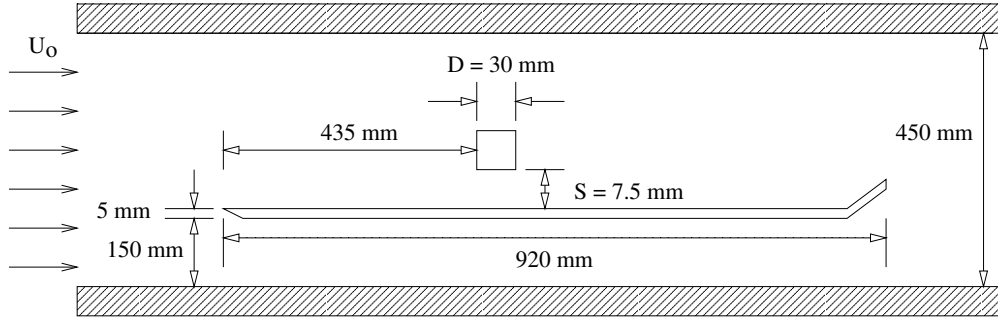


Figure 8. Experimental Set-up

B. Computational domain and sensitivity analysis

The computational domain and boundary conditions are shown in Fig. 9. In the experiment, an end-plate flap was adjusted to maintain parallel flow below the plate. Thus, we assume that the flow above the plate is not influenced by the flow under the plate. Hence, only the portion of the tunnel located above the plate is included in the computational model. Also it was deemed unnecessary to simulate the effect of the end-plate flap.

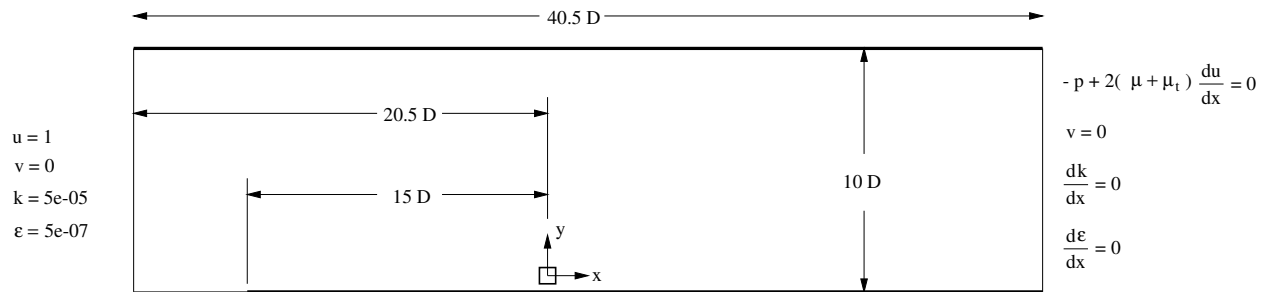


Figure 9. Computational domain and boundary conditions

Wall functions provide boundary conditions along the upper wall of the tunnel, the sides of the obstacles, and the plate. As was shown in a previous paper,²⁴ it is necessary to include the thickness of the real plate in the computational model in order to reproduce the physically observed stagnation point at the leading edge of the plate. The half-thickness of the plate model is therefore set to $0.083D$. With this model geometry, the production of k , which depends on the velocity gradients, is triggered a short distance upstream of the leading edge of the plate so that realistic levels of turbulence are reproduced in this region. The leading edge of the plate, as well as the corners of the cylinder, are rounded to avoid corner singularities with wall functions.

The inlet value of k is set to achieve an inflow with a turbulence intensity of 1%. Based on previous experience,²⁴ the inlet value of ϵ is adjusted so that the inlet eddy-viscosity is equal to ten times the molecular viscosity.

This defines the baseline flow in what follows. For the present sensitivity analysis, we consider the gap size S between the square cylinder and the flat plate as a shape parameter. The baseline configuration is obtained for $S/D = 0.25$. In the remainder, we will only address gap heights for which flows are steady as reported by experimental studies.²³ Hence, we consider only negative variations of the parameter S . That is, a change in the parameter that brings the square cylinder closer to the flat plate. The required sensitivities of geometric quantities are given by :

$$\frac{\partial \hat{n}}{\partial S} = \frac{\partial \hat{t}}{\partial S} = [0, 0]^T \quad ; \quad \frac{\partial \hat{X}}{\partial S} = [0, -1]^T$$

C. Numerical results

The mesh obtained after six cycles of adaptation contains 72276 nodes and is presented in Figure 10. Figure 11 shows closer views of the final adapted mesh. It is refined where the solution fields exhibit rapid variations : near the plate leading edge, along the flat plate, near the square cylinder and in the shear layer emanating from the cylinder corner.

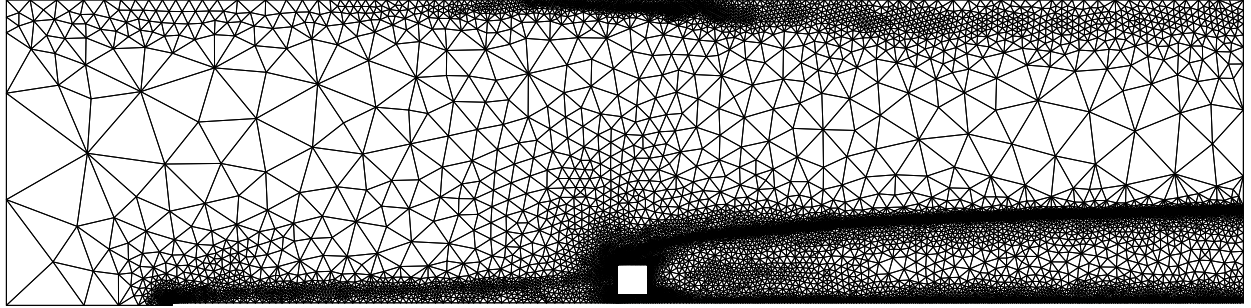


Figure 10. Global view of the final adapted mesh

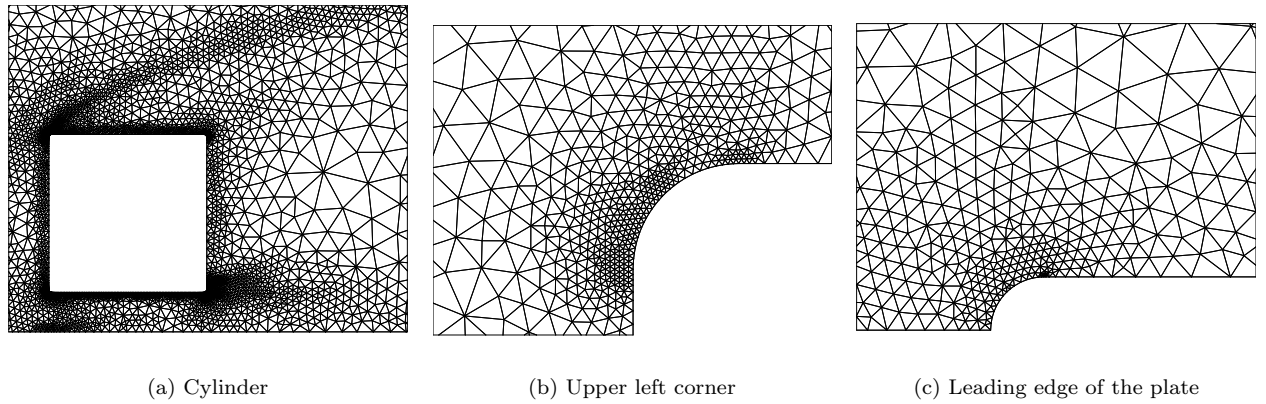


Figure 11. Closer views of the final adapted mesh

The sensitivity fields of the velocity components are shown in Figure 12. They give the trends on how the velocity field will change with the cylinder-to-ground gap size.

To more precisely estimate the accuracy of the computed sensitivity, we now compare the flow solutions obtained by a full flow reanalysis and by Taylor series extrapolation from the baseline flow. Table 3 reports the values of the aerodynamic forces for the two approaches. We have considered two perturbed problems from the baseline flow :

1. 5% of change in S/D : $\Delta S/D = -0.0125$
2. 10% of change in S/D : $\Delta S/D = -0.0125$

As can be seen in Table 3, the extrapolated values are surprisingly accurate even for a reduction of 10% in the gap size. In all cases, the relative differences are much less than the percentage of change from baseline. This confirms the capability of the proposed methodology for computing the material derivatives of integral quantities.

IX. Conclusion

This paper has presented a general Continuous Sensitivity Equation Method for computing shape sensitivities of incompressible turbulent all-bounded flows. The CSE are derived for the RANS equations and the $k - \epsilon$ turbulence model and two-velocity scales wall-functions. The differentiation of the associated boundary

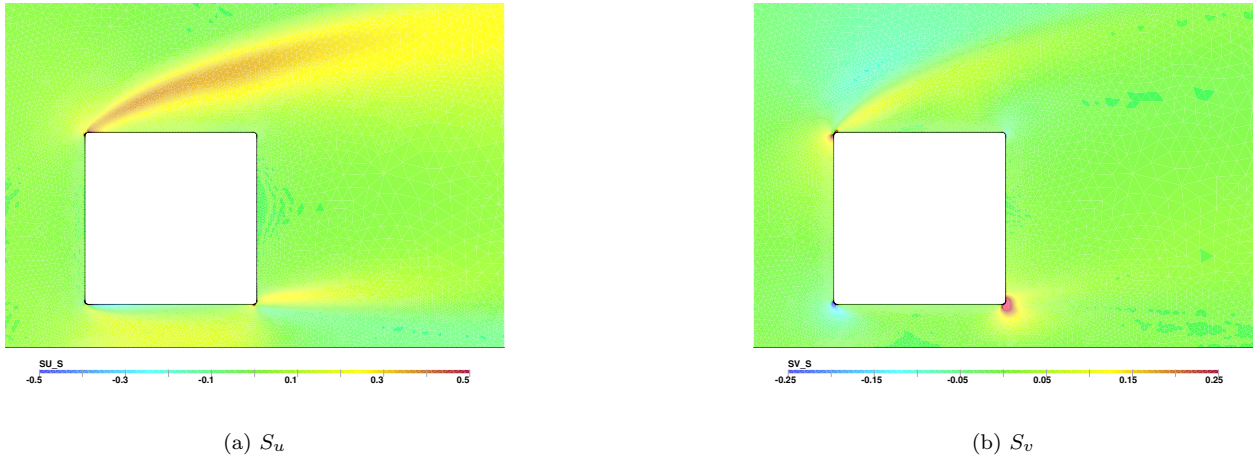


Figure 12. Sensitivity of the velocity components

Configuration	Coeff.	Computed (% Change from baseline)	Extrapolated (% Diff. with computed)
Baseline $(S/D = 0.25)$	F_x	11.419	
	F_y	1.5091	
Perturb 5% $(\Delta S/D = -0.0125)$	F_x	11.520 (0.88%)	11.537 (0.15%)
	F_y	1.5457 (2.42%)	1.5497 (0.26%)
Perturb 10% $(\Delta S/D = -0.025)$	F_x	11.639 (1.93%)	11.654 (0.13%)
	F_y	1.6174 (7.17%)	1.5904 (1.66%)

Table 3. Extrapolation from the baseline flow : integral forces

conditions has been presented in details and accounts for all possible parameter dependencies occurring when shape parameters are considered. The methodology for handling parameter dependent boundaries has been described. Flow and sensitivity solutions were obtained by an adaptive finite-element code. The proposed approach was first verified on a problem with a close form solution. The Method of Manufactured Solutions has allowed us to verify the correctness of the proposed methodology for computing the flow, its sensitivities, and sensitivities of parameter dependent integral quantities such as Friction resistance and aerodynamic coefficients. Finally, the method has been applied to the flow of air around a square cross-section cylinder located in the proximity of a solid wall. Sensitivity analysis with respect to the gap height between the cylinder and the flat plate has been performed. Results show that sensitivity information can be successfully used for fast evaluation of flow for nearby values of the gap. Linear Taylor series in parameter space yield accurate estimates of integrated forces on the square cylinder for perturbations up to 10 % of the gap height.

References

¹Colin, E., Pelletier, D., Borggaard, J., and Etienne, S., "A general sensitivity equation formulation for turbulent heat transfer," *36th AIAA Thermophysics Conference*, Orlando, FL, 23-26 June 2003, AIAA Paper 2003-3636.

²Duvigneau, R., Pelletier, D., and Borggaard, J., "Optimal Shape Design in Mixed Convection Using a Continuous Sensitivity Equation Approach," *38th AIAA Thermophysics Conference*, Toronto, Ontario; Canada, 6-9 June 2005, AIAA Paper 2005-4823.

³Edmond, P., Pelletier, D., Etienne, S., Hay, A., and Borggaard, J., "Application of a sensitivity equation method to compressible subsonic impinging jets," *44th AIAA Aerospace Sciences Meeting and Exhibit*, Reno, NV, January 9-12 2006, AIAA Paper 2006-0909.

⁴Hay, A., Etienne, S., Duvigneau, R., and Pelletier, D., "Evaluation of Flows on Nearby Geometries by a Shape Sensitivity Equation Method," *44th AIAA Aerospace Sciences Meeting and Exhibit*, Reno, NV, 9-12 January 2006, AIAA Paper 2006-1296.

⁵Borggaard, J. and Verma, A., "On Efficient Solutions to the Continuous Sensitivity Equation Using Automatic Differentiation," *SIAM Journal on Scientific Computing*, Vol. 22, No. 1, 2001, pp. 39-62.

- ⁶Duvigneau, R. and Pelletier, D., "On the accuracy of shape parameter boundary conditions in the sensitivity equation method," *43rd AIAA Aerospace Sciences Meeting and Exhibit*, Reno, NV, January 2004, AIAA Paper 2005-0127.
- ⁷Turgeon, É., Pelletier, D., and Borggaard, J., "Application of a Sensitivity Equation Method to the $k - \epsilon$ Model of Turbulence," *15th AIAA Computational Fluid Dynamics Conference*, Anaheim, CA, Jun. 2001, AIAA Paper 2001-2534.
- ⁸Turgeon, É., Pelletier, D., and Borggaard, J., "A General Continuous Sensitivity Equation Formulation for the $k - \epsilon$ Model of Turbulence," *31st AIAA Fluid Dynamics Conference and Exhibit*, Anaheim, CA, Jun. 2001, AIAA Paper 2001-3000.
- ⁹Turgeon, É., Pelletier, D., and Borggaard, J., "Computation of Airfoil Flow Derivatives Using a Continuous Sensitivity Equation Method," *8th CASI Aerodynamics Symposium*, Toronto, Canada, April 2001.
- ¹⁰Pelletier, D., Turgeon, É., Etienne, S., and Borggaard, J., "Reliable Sensitivity Analysis Via an Adaptive Sensitivity Equation method," *3rd AIAA Theoretical Fluid Mechanics Meeting*, St Louis, MO, Jun. 2002, AIAA Paper 2002-2758.
- ¹¹Roache, P. J., *Verification and Validation in Computational Science and Engineering*, Hermosa publishers, Albuquerque, NM, 1998.
- ¹²Ilinca, F. and Pelletier, D., "Positivity Preservation and Adaptive Solution for the $k - \epsilon$ Model of Turbulence," *AIAA Journal*, Vol. 36, No. 1, 1998, pp. 44–51.
- ¹³Lauder, B. E. and Spalding, J., "The Numerical Computation of Turbulent Flows," *Computer Methods in Applied Mechanics and Engineering*, 1974, pp. 269–289.
- ¹⁴Chabard, J.-P., "Projet N3S - Manuel de la version 3," 1991, Tech. Rep. EDF HE-41/91.30B, Electricité de France.
- ¹⁵Ignat, L., Pelletier, D., and Ilinca, F., "Adaptive Computation of Turbulent Forced Convection," *Numerical Heat Transfer, Part A*, Vol. 34, 1998, pp. 847–871.
- ¹⁶Schetz, J., *Boundary Layer Analysis*, Prentice Hall, 1993.
- ¹⁷Brooks, A. N. and Hughes, T. J. R., "Streamline Upwind/Petrov-Galerkin formulations for convection dominated flows with particular emphasis on the incompressible Navier-Stokes equations," *Computer Methods in Applied Mechanics and Engineering*, Vol. 32, 1982, pp. 199–259.
- ¹⁸Ilinca, F., Hétu, J.-F., and Pelletier, D., "On stabilized finite element formulations for incompressible advective-diffusive transport and fluid flow problems," *Computer Methods in Applied Mechanics and Engineering*, Vol. 188, No. 1, 2000, pp. 235–257.
- ¹⁹Pelletier, D., "Adaptive Finite Element Computations of Complex Flows," *International Journal for Numerical Methods in Fluids*, Vol. 31, 1999, pp. 189–202.
- ²⁰Eça, L., Hoekstra, M., Hay, A., and Pelletier, D., "A Manufactured Solution for a two-dimensional steady wall-bounded incompressible turbulent flow," *7th World Congress on Computational Mechanics, Accomplishments and Challenges in Verification & Validation*, Los Angeles, July 2006.
- ²¹L. Eça, M. Hoekstra, A. H. and Pelletier, D., "Verification of RANS solvers with Manufactured Solutions," 2006, Submitted to Engineering with computers.
- ²²Hay, A. and Pelletier, D., "Second Workshop on CFD Uncertainty Analysis : Results from the CADYF code," *2nd Workshop on CFD Uncertainty Analysis*, Lisboa, Portugal, October 2006.
- ²³Wu, K. and Martinuzzi, R., "Experimental study of the turbulent wake flow behind a square cylinder near a wall," *ASME Fluids Engineering Division*, Vancouver, B.C., June 22–26 1997, No. FEDSM97-3151.
- ²⁴Lacasse, D., Turgeon, É., and Pelletier, D., "On the Judicious Use of the $k - \epsilon$ Model, Wall Functions and Adaptivity," *39th AIAA Aerospace Sciences Meeting and Exhibit*, Reno, NV, Jan. 2001, AIAA Paper 2001-0882.